




Research Article

Influence of acid pretreatment on the hydrodeoxygenation performance of carbon supported RuMo bimetallic catalysts on sorbitol conversion

Longlong Wang^{1,2} · Yujing Weng^{1,2}  · Peigao Duan¹ · Xianyun Liu¹ · Xiaolong Wang¹ · Yulong Zhang^{1,2} · Chenguang Wang³ · Qiying Liu³ · Longlong Ma³

© Springer Nature Switzerland AG 2019

Abstract

Sorbitol was reported as one promising platform compounds as a C6 sugar related derivative from biomass cellulose due to its high oxygen content with six hydroxyl groups. Our previous work has reported the selective hydrodeoxygenation (HDO) of sorbitol into long alkanes such as pentane and hexane (C5/C6) over carbon supported ruthenium-molybdenum catalysts. Here, the effect of acidic pretreatments of those carbon catalysts on the performance of HDO reaction was studied in detailed. The result indicated that carbon support pretreated by phosphoric acid presented much phosphorus groups, but the carbon support pretreated by nitric acid presented high graphitization degree. Moreover, the phosphoric acid pretreated catalyst (RuMo/C-P) obtained high HDO performance in the sorbitol conversion with 79.7% carbon yield of C5/C6 alkane (pentane and hexane). Finally, detailed characterizations (N₂-adsorption, XRD, HRTEM, XPS, XRF, Raman, NH₃-TPD, Py-IR spectrums, etc.) were performed over relevant catalysts for correlating their catalytic and physicochemical properties.

Keywords Biomass conversion · Renewable alkanes · Hydrodeoxygenation · Ruthenium–Molybdenum catalyst · Carbon pretreatment

1 Introduction

Fuels and valued-chemicals from biomass resource are most important topics in green chemistry, based on the fact that biomass is the only promising alternative carbon resource. The challenge to reconstitute biomass resources is their polyoxygenated nature (CHO)_n, which requires the transformation of C–O bond for oxygen removal or substitution [1–3]. However, the thermodynamic data showed that the bond-dissociation for C–O bonds (CH₃–OH 381 kJ/mol, CH₃CH₂–OH 381 kJ/mol, CH₃CH₂CH₂–OH 381 kJ/mol)

were higher than that of C–C bonds (CH₃–CH₃ 368 kJ/mol, CH₃CH₂–CH₃ 356 kJ/mol, CH₃CH₂–CH₂CH₃ 381 kJ/mol) [4–6]. Thus, the control of relative activity in cracking reaction of C–C and C–O bonds is one of the most important themes of the design of hydrodeoxygenation catalysts as most metal catalysts can crack both C–C and C–O bonds [7, 8].

Recently, bimetallic metal/metal-oxide catalysts have been shown to be very promising for the catalytic HDO of biomass-derived oxygenates into valued chemicals and fuels. Tomishige et al. [2] reported Ir–ReO_x catalysts for the

Electronic supplementary material The online version of this article (<https://doi.org/10.1007/s42452-019-0434-3>) contains supplementary material, which is available to authorized users.

✉ Yujing Weng, wengyj@hpu.edu.cn; ✉ Yulong Zhang, zhangyulong@hpu.edu.cn; ✉ Longlong Ma, mall@ms.giec.ac.cn | ¹Henan Polytechnic University, Jiaozuo 454003, Henan, People's Republic of China. ²Henan Key Laboratory of Coal Green Conversion, Henan Polytechnic University, Jiaozuo 454003, Henan, People's Republic of China. ³Key Laboratory of Renewable Energy, Guangzhou Institute of Energy Conversion, Chinese Academy of Sciences, Guangzhou 510640, People's Republic of China.



SN Applied Sciences (2019) 1:404 | <https://doi.org/10.1007/s42452-019-0434-3>

Received: 13 February 2019 / Accepted: 29 March 2019 / Published online: 4 April 2019

SN Applied Sciences
A SPRINGER NATURE journal

conversion of biomass derivatives into bio-alkanes, and found that the Re species played critical role in the synergistic HDO process [9–11]. Huber et al. reported bimetallic Pt-ReO_x catalyst for biomass sugar and polyol into bio-alkanes and -alcohols [12–16]. Chemically speaking, those catalysts presented metal/acid bifunctional catalytic roles. The metal sites can catalyze the hydrogen uptake, dissociation and spillover onto the metal-oxide in vicinity. It was generally believed that H₂ spillover can facilitate the reduction of metal-oxide species. Moreover, the reduced metal-oxide species can act as Lewis acid sites for the C–O bond cracking via dehydration reaction [17–20].

Our group aimed to directly convert biomass into renewable alkanes on trickle-bed reactor over carbon supported Ru–Mo bimetallic catalyst due to the relative cheap and hydrothermal stability of materials. To date, several attempts have been made to optimize the hydrodeoxygenation performance over carbon supported catalysts, such as adjusting the Ru/Mo composition and screening additives [21–25]. The purpose of this study was to investigate the influence of acid pretreatment on physicochemical properties and hydrodeoxygenation performance of carbon supported Ru–Mo bimetallic catalysts. Wherein, activated carbons prepared by chemical activation using nitric acid and phosphoric acid contain a relatively higher amount of nitrous or phosphorus complex, which could achieve the desired properties such as high oxidation resistance and high surface acidity [26–29]. In addition, such carbon supported catalysts have been successfully used as acid catalysts in the dehydration reactions [12, 29, 30].

Here, RuMo/C catalysts prepared from impregnation by using different acid pretreated activated carbon were employed and extensively studied in trickle-bed reactor for sorbitol conversion. Among these catalysts, the best HDO performance was approximately 80% carbon yield of C5/C6 alkane, but the inferior HDO performance was only about 55% carbon yield of C5/C6 alkane. Thus, it is worthwhile to explore the influence of carbon pretreatment. Subsequently, a series of characterization studies (N₂-adsorption, XRD, XRF, HRTEM, XPS, Raman, H₂-TPR, NH₃-TPD, Py-IR spectrums, etc.) were performed over relevant catalysts to study the catalytic and physicochemical properties.

2 Experimental

2.1 Materials

Sorbitol was supported by Yuan-Ju biotechnology Reagent Co. Ltd. (Shanghai, China). Ruthenium-chloride-hydrate (RuCl₃·3H₂O), nitric acid (HNO₃, 68 wt%) and phosphoric acid (H₃PO₄, 85 wt%) were supplied by

Aladdin Co. Ltd. (Shanghai, China). Hexaammonium-molybdate ((NH₄)₆Mo₇O₂₄), diammonium hydrogen phosphate ((NH₄)₂HPO₄), and melamine (C₃H₆N₆) were purchased from Tianjin Fuyu Fine Chemical Co. Ltd. (Tianjin, China). Activated carbon (AC, 70–120 mesh, Huaneng carbon Co., Ltd., Hebei, China), multi-walled carbon nanotube (CNT, inner diameter 2–5 nm, length 10–30 μm, Chengdu Organic Chemicals Co., Ltd., Chinese Academy of Sciences, Sichuan, China) and graphene (GC, thickness 0.55–3.74 nm, Chengdu Organic Chemicals Co., Ltd., Chinese Academy of Sciences, Sichuan, China) were selected as support materials.

Ruthenium molybdenum carbon catalysts were prepared by sequential impregnation with 1.5 wt% Ru loading amount and molar ratio of Ru/Mo = 1 (Fig. S1). Take the RuMo/C–P catalyst as an example. Firstly, activated carbon needed to be pretreated by phosphoric acid at 383 K in condensing reflux equipment overnight, then cooled to RT, filtered and dried at 393 K overnight before impregnation. Secondly, the activated carbon was immersed into RuCl₃ solution followed by ultrasonic treatment for 2 h and incipient impregnation. Thirdly, the mixture was then transferred to an oven and dried at 393 K for 12 h, the dry sample was next heat treated in a muffle furnace under a nitrogen atmosphere at 673 K for 4 h. Finally, the impregnation of Mo was carried out in the similar process. RuMo/C–N catalyst followed the sample process but selected the nitric acid for pretreatment of activated carbon. Additionally, all catalysts needed to be reduced in a H₂ flow (150 cm³/min) at 673 K for 4 h prior to the reaction.

2.2 Characterization

The adsorption properties of catalysts were characterized by nitrogen adsorption at 77 K. To further determine the surface properties of fresh and spent catalysts, Fourier transform infrared spectroscopy (FT-IR), X-ray diffraction (XRD), X-ray fluorescence (XRF), Raman spectra, X-ray photoelectron spectroscopy (XPS), transmission electron microscopy (TEM), H₂ temperature-programmed reduction (H₂-TPR), NH₃ temperature-programmed desorption (NH₃-TPD) and infrared spectra of pyridine adsorption (Py-IR) were also employed. Moreover, detailed characterization information was supported in supplementary materials.

2.3 Catalyst test and product analysis

Sorbitol conversion was carried out in a tubular stainless-steel trickle-bed reactor (inner diameter of 10 mm; length of 350 mm) with 4 MPa H₂ pressure. Before the reaction, 4 ml catalyst was located in the constant temperature zone of the reactor and certain amount of quartz sand

and quartz wool were loaded on the top and bottom of the catalyst bed as the filler materials, respectively. During the reaction, sorbitol solution (20 wt%) was pumped into the reactor at different flow rate by a high-pressure liquid pump (HPLP), and H_2 flow (150 cm^3/min) was purged at the same time. The set-up kept H_2 pressure at 4 MPa with the use of pre-pressure controller and rear pressure and operated in the co-current-flow from top to bottom.

The products here were distributed in gaseous phase and liquid phase. Where, Gaseous sample was analyzed on-line by gas chromatography (Shimadzu GC-2010, Rt@-Alumina Bond capillary column, 50 m \times 0.53 mm, \pm 5%) equipped with a thermal conduct detector (TCD) and a flame ionization detector (FID) via external standard method. Moreover, liquid samples were condensed and collected in an ice-water condensing tank and then weighted at Analytical Balance (\pm 0.5%), further detected by Waters Alliance e2695 HPLC (\pm 2.27%) with UV-Vis (Waters 2489) and Refractometer (Waters 2414) detector by using a Shodex SH1011 column (8 \times 300 mm). 0.005 M H_2SO_4 as mobile phase flowed at a rate of 0.5 ml/min. GC-MS (Thermo Trace GC Ultra with a Polaris-Q ion trap mass spectrometer) equipped with a HP-INOWx capillary column was applied to analyze the species in aqueous samples. The total carbon content in the liquid products was measured by a Vario EL III elemental analyzer (\pm 0.2%).

3 Results and discussion

3.1 Catalyst characterization

Figure 1 showed the N_2 adsorption-desorption isotherms at $-196^\circ C$ for the different pretreated carbon catalysts.

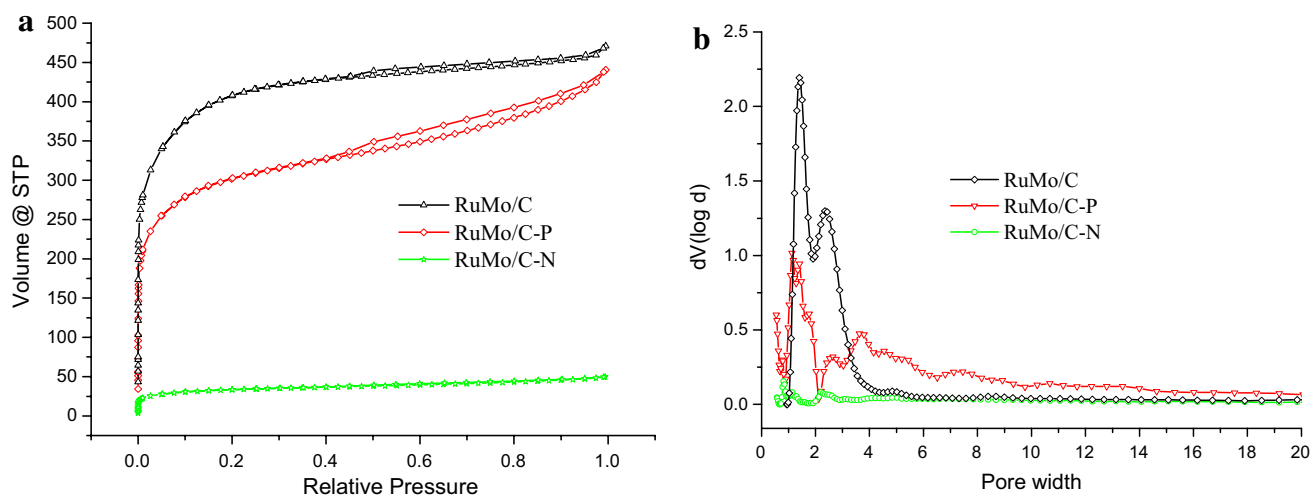


Fig. 1 a N_2 adsorption-desorption isotherms and b pore size distribution curves

Moreover, quenched solid density functional theory (QSDFT) method was applied to analysis the heterogeneous samples, which allows reliable pore size, porosity and surface area characteristics to be calculated in the pore width range from micropore to mesoporous (0.35 to 40.0 nm) [31]. RuMo/C presented a type IV isotherm, corresponding to a well-developed micro- and mesoporous structure, as a large amount of N_2 was adsorbed in the entire relative pressure range, which was further confirmed by the higher surface areas (S_{BET} , 1500 m^2/g) and larger pore volume (V_p , 0.73 cm^3/g) in the Table 1. The heterogeneous porous property would facilitate the chemisorption and dispersion of metal particles according to relevant literature [32]. For RuMo/C-P catalyst, the value of S_{BET} and V_p slightly decreased. As to RuMo/C-N, a great reduce of micropore and mesoporous was found with only 122 m^2/g surface area and 0.07 cm^3/g total pore volume. Cordero et al. reported that the nitration of activated carbon with nitric acid would result to a decrease of porosity [27, 29, 33, 34].

Pretreatment carbon with nitric acid or phosphoric acid was a typical method, not only introducing oxygen-surface groups on the carbon support but also introducing a small amount of nitrogen or phosphate functional

Table 1 Structural characteristic of the catalyst samples

Sample	S_{BET} (m^2/g)	V_p (cm^3/g)	A_t (m^2/g)	V_{mes} (cm^3/g)
RuMo/C	1500	0.73	163	0.16
RuMo/C-P	1110	0.61	144	0.55
RuMo/C-N	122	0.07	90	0.03

S_{BET} the apparent surface area, V_p the total pore volume, A_t the external surface area and V_{mes} mesoporous volume

groups. Thus, the detailed elemental analysis of pre-treated carbons by XRF was presented in Table 2. For the carbon pretreated by H₂O, a large amount of C, O, Cl, Ca, Si, a small amount of K, Fe, Al, P, Mg, and a trace amount of S, Ti, Na, Ba, Mn, Cu were detected, which were the mostly frequent and abundant mineral elements in natural carbon materials according to reports [35, 36]. Moreover, the mineral elements were decreased for the carbon pre-treated by acid solutions, especial the one using HNO₃. Interestingly, the carbon pre-treated by HNO₃ presented very trace amount of N element (0.001%) on the support, but the carbon pre-treated by H₃PO₄ showed a large amount of P element (3.005%). According to previous reports, the presence of P element could be attributed to the surface phosphorus complexes formed during the activation step, which seem to be stably bonded to carbon as they do not elute after washing and ultrasonic processes [35, 36].

XRD analysis was also carried out to investigate the structure of catalysts in Fig. S2. Unfortunately, no obvious difference was observed among the catalysts due to the amorphous property of AC and fine particles size [23, 31, 37]. Moreover, Raman spectra of samples were also supported in Fig. 2. The spectra of ordinary carbon materials exhibited a D band around 1360 cm⁻¹ due to the

disordered arrangement and low symmetry of graphite lattice structure. An additional G band at around 1580 cm⁻¹ is a scattering peak attributed to the stretching of all sp² atomic pairs on carbon ring or long carbon-chain in graphite. The value of L_a ($R = I_D/I_G$, $L_a = 44/R$) was calculated in Table S1 to characterize the degree of graphitization level. The L_a value of RuMo/C, RuMo/C-P and RuMo/C-N were 20.9, 21.6 and 22.4, respectively, indicated the acid pre-treatment enhance the graphitization of carbon catalysts.

To further identify the chemical states of relevant catalysts, XPS was employed with Gaussian-Lorentzian peak shapes as fitting method and Shirley line as background. Figure 3a showed the spectrum of C1s region. The main occurrence in samples could be attributed the species of Csp³ (aliphatic carbon in hydrocarbonates, C-C-, O-C-, etc.) and Csp² (-C=O, -C=C, etc.). Figure 3b confirmed the presence of several different O species in the O1s region: (1) 529.2–530.6 eV (metal oxides, Mo-O), (2) 531.0–531.9 eV (C=O, O-C=O*, P-O), (3) 532.0–534.5 eV (C-OH, C-O-C, *O-C=O), (4) 534.5–536.1 eV (H₂O) [25, 31]. Figure 3c showed the Ru3p spectra. Whereby, the main peak (based on Ru 3p_{3/2}) at around 462.3 eV observed on catalysts could be attributed to the metallic Ru (Ru⁰) and the broad band at around 464.0 eV could be corresponded to high valance of RuO_x species according to relevant reports [38, 39]. Figure 3d presented the Mo3d spectra. The high binding energy peaks at around 233.6 eV could be attributed to the Mo⁶⁺ species and the lower binding energy peaks at around 232.0 eV could be assigned to the reduced metal oxide species (MoO₂). Moreover, P2p and N1s spectra of relevant catalysts were also supported in the Fig. S4. A broad band at around 133.0 eV in P2p spectra reflected the reduced P species (e.g., C-PO₃ and C₂-PO₂ 133.1 eV) and the other smaller band at around 134.4 eV could be corresponded to P (+V) species (e.g., H₂PO₄⁻ 134.6 eV). While, the peaks at around 399.0 eV in N1s spectra suggested the appearance of reduced N

Table 2 The elemental analysis of pre-treated carbon support by XRF

Entry	Element/ %	H ₂ O	HNO ₃	H ₃ PO ₄
1	C	86.043	89.423	85.456
2	O	5.265	5.589	5.759
3	Cl	3.284	2.530	2.709
4	Ca	2.265	0.376	0.457
5	Si	1.003	0.945	1.151
6	K	0.653	0.426	0.626
7	Fe	0.615	0.385	0.345
8	Al	0.252	0.118	0.148
9	P	0.231	0.015	3.055
10	Mg	0.138	0.040	0.025
11	S	0.066	0.042	0.105
12	Ti	0.053	0.039	0.072
13	Na	0.047	0.021	0.028
14	Ba	0.027	0.015	0.025
15	Mn	0.022	0.008	0.008
16	Cu	0.011	0.008	0.011
17	Br	0.007	0.006	0.004
18	Sr	0.006	0.006	0.006
19	Ni	0.005	0.003	0.005
20	Zn	0.005	0.004	0.005
21	Ga	0.002	/	/
22	N	/	0.001	/

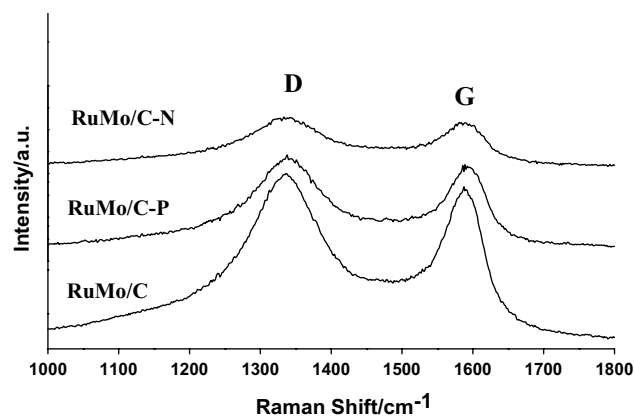


Fig. 2 Raman spectra of relevant catalysts

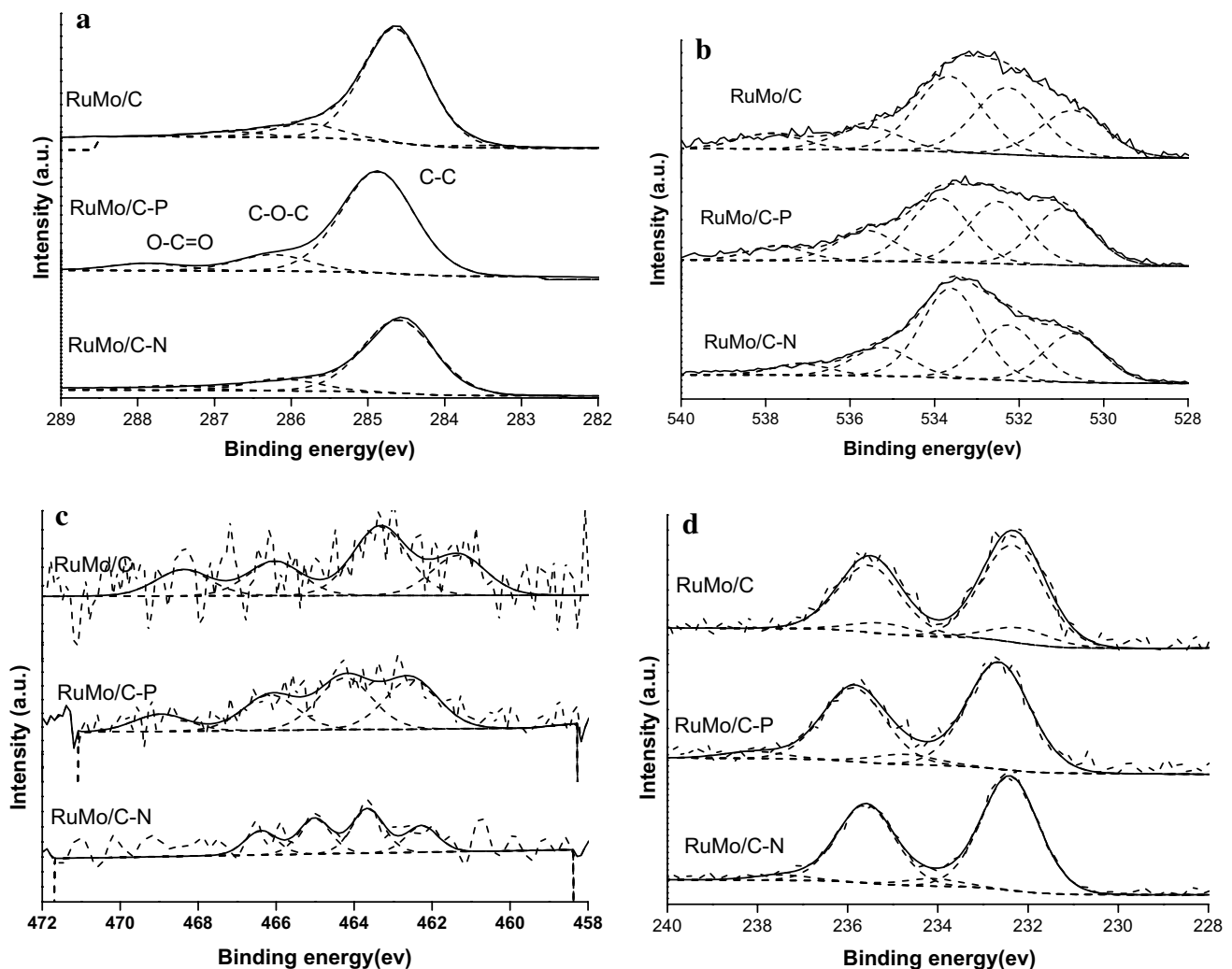


Fig. 3 XPS spectra of spent samples **a** C1s, **b** O1s, **c** Ru3p and **d** Mo3d

species (e.g., nitroso 400.1 eV, pyridinic 398.9 eV) according to reported literature [27].

TEM experiments were conducted to study the dispersion of metal particles. As shown in Fig. 4a–c, the RuMo/C catalyst presented a good dispersion of metal particles with an average size about 3.4 nm, which could be the result of high surface area and pore volume. But better nanoparticle dispersion with average size about 1.9 nm and 1.0 nm was also found on the catalyst after acid pretreatment on RuMo/C–P (Fig. 4d–f) and RuMo/C–N (Fig. 4g–i) samples, respectively. Although the N₂ adsorption–desorption characterization suggested the change of carbon microstructure of supports after acid pretreatment, the TEM results still showed high dispersion of nanoparticle on relevant catalysts.

The TPR profiles of series catalysts were conducted to provide further evidence for the change of activity sites. The comparison of RuMo/C with those of Ru/C, Mo/C and

AC itself was supported in Fig. S5. Ru/C showed a main peak below 400 °C, and Mo/C gave a big peak above 500 °C. While, RuMo/C presented a big peak located at a slightly higher temperature than that of Ru/C catalyst, and the peak assignable to Mo species was nearly disappeared, which suggested that the reduction of Mo species could be promoted by the presence of Ru via H₂ spillover [17, 20, 21, 23, 40]. The evaluated value of Mo species based on the H₂ consumption was determined about +4, which was also supported by XPS result. Moreover, Fig. 5 showed the TPR profiles of RuMo catalysts. RuMo/C–P showed a low temperature broad peak was at the range of 150–400 °C, and a high broad peak evolving at above 500 °C. RuMo/C–N also presented a low temperature peak was at the range of 200–400 °C, and a high broad peak evolving at above 500 °C. Generally, the low temperature peak could be attributed to the reduction of RuO_x and MoO_x species, and the high temperature peak could be assigned to the

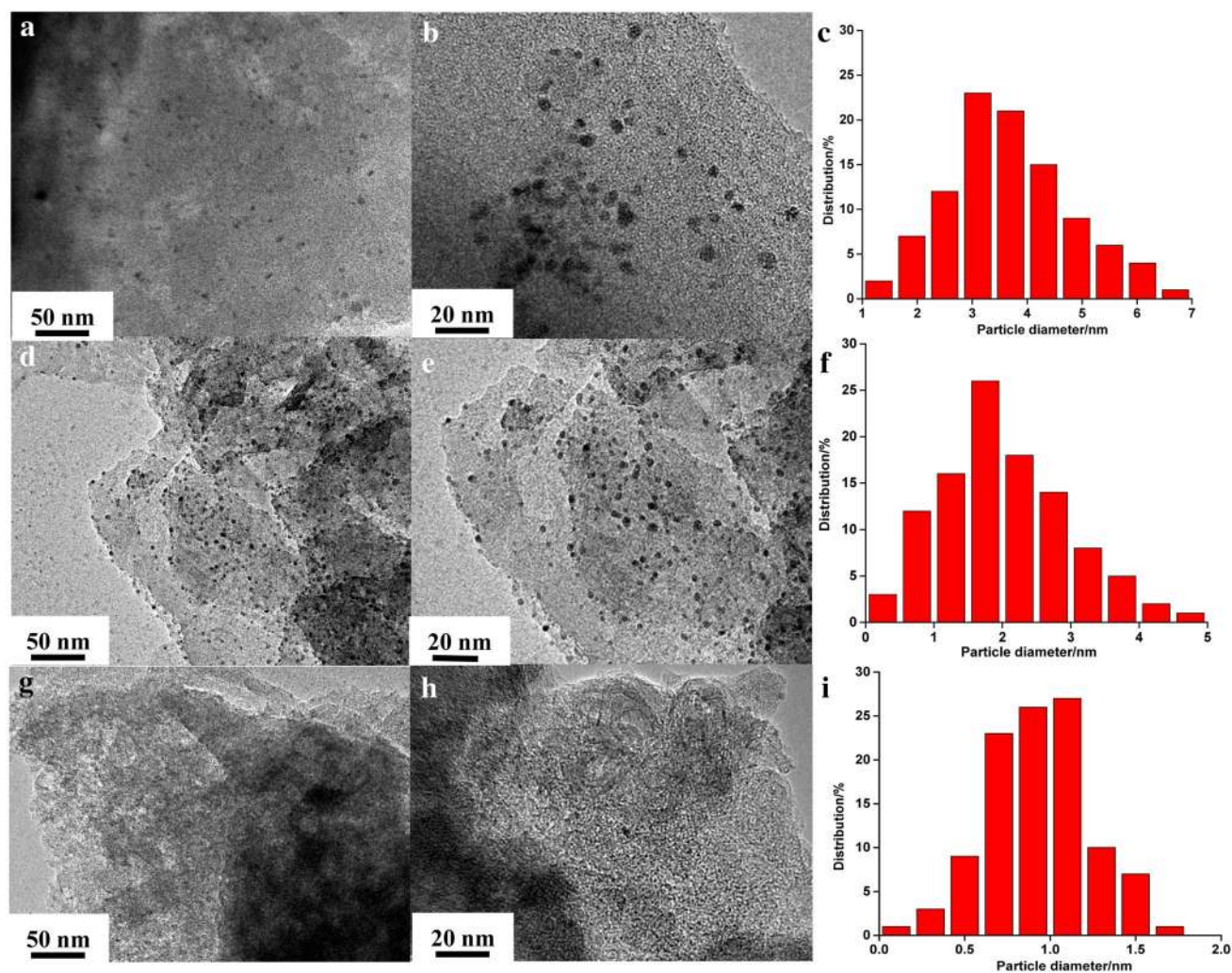


Fig. 4 Representative TEM images and corresponding particle distribution of RuMo/C (**a–c**), RuMo/C–P (**d–f**) and RuMo/C–N (**g–i**) catalysts

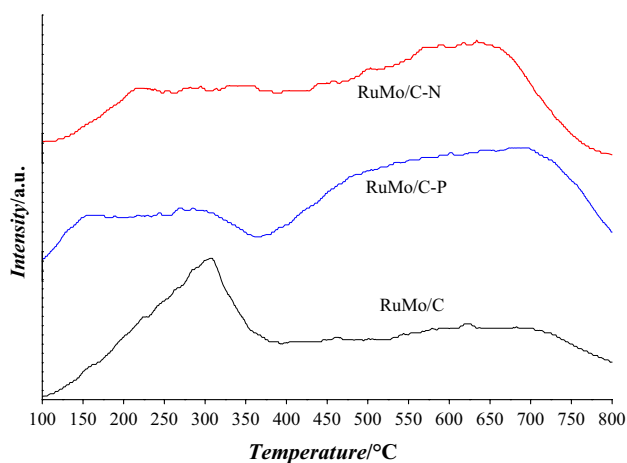


Fig. 5 H₂-TPR profiles of RuMo catalysts

decomposition of oxygenate-containing groups [22, 25]. Obviously, the range of these peaks did not overlap with RuMo/C catalyst, indicating that the reducibility of RuMo bimetallic catalyst was affected by the acid pretreatment of carbon supports.

Acid pretreatment would enhance the acid character of carbon catalysts, which rendered them interesting catalytic properties and has been already reported in the previous works [24, 25]. Here, surface acidity of catalysts was evaluated by NH₃-TPD. As shown in Fig. S6, all catalysts presented weak-medium acidity with two distinct NH₃ desorption peaks at around 420 and 570 K [41]. To further investigate the percentage of Brønsted (B) and Lewis (L) acid sites in the total number of acid sites, the spent samples were measured by Py-IR spectroscopy at different desorption temperatures (Table 3). Chemically speaking, the Brønsted acid sites could be attributed to

the hydroxy groups on the support and easy to be dissociated at high temperature. While, the reduced Mo species can act as Lewis acid sites or electrophilic sites to polarize and facilitate the cleavage of C–O bond [2, 17, 20, 42].

4 Catalytic performance

Ru-based catalysts were well known to be active in the aqueous-phase catalytic transformation of biomass feedstocks, and our previous work have reported the selective HDO of sorbitol into C5/C6 alkane over carbon supported ruthenium-molybdenum catalysts, which presented excellent stability for 7 days without obvious decline (Fig. S7) [21–25, 31]. Here, the effect of carbon pretreatments were studied in detailed. As shown in Table 4, all ruthenium-molybdenum catalysts exhibited low selectivity to short alkanes and high selectivity to long alkanes, indicated higher HDO performance than that of monometallic Ru/C catalyst. Whereby, RuMo/C showed stable HDO performance with 62.6, 68.5 and 66.3% yields to C5/C6 alkanes at 280, 300 and 320 °C, respectively. RuMo/C–P also presented lower C–C cracking property with high C5/C6 alkanes yields of 70.4, 74.2 and 79.7% at 280, 300 and 320 °C, respectively. However, RuMo/C–N presented inferior performance in the cleavage of C–O versus C–C bond with 62.2, 57.9 and 55.0% yields to C5/C6 alkanes at 280, 300 and 320 °C,

respectively. Thus, those results indicated that the acid pretreatment of carbon supports can affected the HDO performance of relevant RuMo catalysts. Generally, it was supposed that the selective of C–O/C–C bond cleavage was attributed to the bimetallic Ru–MoO_x structure on catalyst which suppressed the C–C cracking reaction and enhanced the HDO performance [23].

Furthermore, the activity test of monometallic Ru catalysts supported on various carbon materials was also carried out to study the effect of acid pretreatment. As shown in Table S2, the result suggested that the acid pretreatment can affected the C–C cracking performance of Ru catalysts with relative low yield of C1 products. As mentioned in XRF results, acid pretreatment introduced a small amount of P and N element. Thus, nitrogen and phosphorus additives were added into the Ru/C catalysts for comparative study (Table S2). For the catalyst with phosphorus additive, the selectivity for C5/C6 alkane was about 50%, slightly lower to that of monometallic Ru on phosphoric acid pretreated carbon support (Ru/C–P). While, it still presented similar products distribution with high selectivity to C1 products for the catalyst with nitrogen additive. Thus, the result indicated that the phosphorus additive has an inhibitory effect on the crack property of Ru metal.

Since graphitization was detected on catalyst after nitric acid pretreatment, graphitized carbon materials [carbon nanotube (CNT) and graphene (GC)] were employed as supports to prepare ruthenium molybdenum bimetallic

Table 3 Acidity of these catalysts obtained by Py-IR

Catalyst	40°C ^a		100°C ^a		280°C ^a	
	B (umol/g)	L (umol/g)	B (umol/g)	L (umol/g)	B (umol/g)	L (umol/g)
RuMo/C	2.8	10.8	2.2	9.6	1.1	7.2
RuMo/C–P	3.0	13.2	2.3	8.4	1.2	6.4
RuMo/C–N	2.5	13.2	1.8	10.8	0.8	9.6

^aDesorption temperatures of pyridine (Py)

Table 4 Effect of mineral acids of pre-treatment on the sorbitol conversion

Acid ^a	Tem. (K)	Conv. (%)	Yield (%)							Carbon Balance (%)
			C1	C2	C3	C4	C5	C6	Others	
RuMo/C	553	91.6	9.3	2.3	3.9	7.3	27.2	35.4	2.0	87.4
RuMo/C	573	99>	10.8	2.7	4.3	9.2	29.7	38.8	/	95.5
RuMo/C	593	99>	11.0	2.9	6.2	9.7	29.4	36.9	/	96.1
RuMo/C–N	553	96.8	13.7	3.6	5.4	10.4	23.3	38.9	1.0	96.3
RuMo/C–N	573	99>	18.3	3.6	7.5	10.8	20.8	37.1	0.1	98.1
RuMo/C–N	593	99>	19.7	4.6	8.9	11.8	21.4	33.6	/	100
RuMo/C–P	553	99>	9.8	4.2	5.3	9.9	35.1	35.3	0.2	99.8
RuMo/C–P	573	99>	9.3	3.0	4.0	8.6	32.3	41.9	/	99.1
RuMo/C–P	593	99>	5.2	3.2	3.9	6.7	32.6	47.1	/	98.7

^aCatalysts using different carbon pre-treated acid solution. Reaction conditions, temperature 573 K, 4 MPa H₂ pressure, GHSV = 2250 h⁻¹, 20 wt% sorbitol solution, LHSV = 0.75 h⁻¹, 4 ml catalyst, /, trace

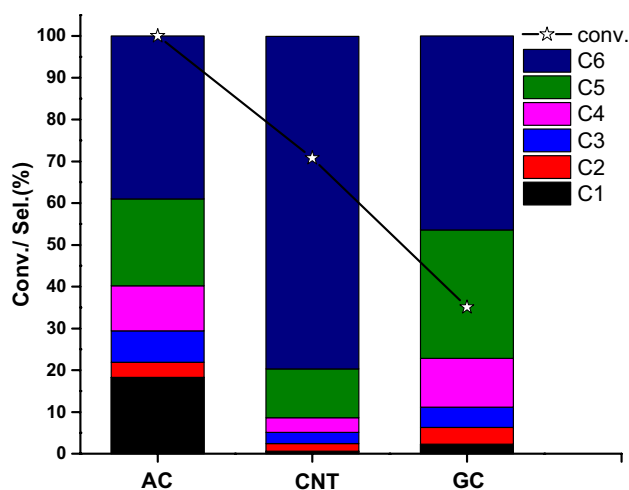


Fig. 6 Comparison of catalytic performance of RuMo bimetallic catalysts with different carbon supports under the reaction temperature 573 K, 4 MPa H₂ pressure, GHSV=2250 h⁻¹, 20 wt % sorbitol solution, LHSV=0.75 h⁻¹

catalysts to further study the effect of graphitization on catalytic mechanism. Figure 6 showed the result of products distribution over catalysts with different supports. As expected, the sorbitol conversions and products distribution were influenced by the carbon materials. The CNT supported catalyst showed 70.8% sorbitol conversion and 91.3% carbon selectivity to C5/C6 alkanes in the gaseous products. While, the GC supported catalyst showed 35.1% sorbitol conversion and 77.2% carbon selectivity to C5/C6 alkanes in the gaseous products. The comparison here was at fixed catalyst volume. Thus, much less catalysts were used as the lower density of CNT and GC materials than that of AC material, which could result to low conversion at same sorbitol LHSV. Therefore, the result indicated that graphitized carbon supports have no suppression effect on the HDO performance of Ru–Mo bimetallic catalysts. Furthermore, relevant characterization of RuMo/CNT catalyst was supported in Fig. S8.

5 Catalysts comparison and mechanism study

HDO is a catalytic process to remove partial or total oxygenates from biomass feedstock, which involved at least the C–O bond cleavage by dehydration at acid sites and the hydrogenation of C=C and C=O bonds at metal sites. Side-reactions included the C–C bond cleavage by dehydrogenation followed by decarbonylation or retro-aldol condensation at metal sites. Thus, active and stable acid/metal bifunctional catalysts were needed. According to the result of characterization and previous reports, Ru–MoOx

structure here was that Ru species are in the metallic state acted as metal sites on catalyst with nanoscale dispersion, and Mo species are partially reduced to a low valence and acted as acid sites [3, 22, 43, 44]. Moreover, the intimate contact between Ru and Mo species would enhance the synergistic effect. However, the C–C bond cleavage of Ru-based catalysts at high reaction temperatures was still challenging.

The purpose of this study was to investigate the influence of acid pretreatment on the physicochemical properties and HDO performance of carbon supported Ru–Mo catalysts [12, 36, 45–47]. Whereby, RuMo/C–P catalyst presented a high selectivity to C5/C6 alkane, suggesting the low C–C cracking property of catalyst. Relevant characterizations indicated the introduction of P groups on catalyst, which enhanced the acidity of catalyst, especially the Brønsted acid. Moreover, contrast experiment also suggested that the reduced P groups could affect the chemical state of Ru and low the cracking property of catalyst [48–51]. However, the effect of nitric acid pretreatment was much complex. Whereby, change of porous structure, graphitization of carbon support and reduced N groups were detected. Current work could just confirm that the graphitized carbon supports have no negative effect on the HDO performance of RuMo catalyst. Since the complex of carbon materials and challenge of in situ analysis for aqueous HDO catalytic system at present, detailed synergy catalytic mechanism will be further studied in future.

6 Conclusions

In this work, Ru–Mo bimetallic catalysts prepared by using different acid pretreated carbon supports were employed in continuous trickle-bed reactor for hydrodeoxygenation of biomass sorbitol into renewable alkanes. The result indicated that the sorbitol conversion and products distribution were seriously influenced by the carbon pretreatment during impregnation. The best obtained HDO performance was approximately 80% carbon yield of C5/C6 alkane, but the inferior HDO performance was only about 55% carbon yield of C5/C6 alkane. Therefore, a series of characterization studies were performed over relevant catalysts to study the change of catalytic active sites. The result indicated that carbon support pretreated by phosphoric acid presented more phosphorus groups, which enhanced the acidity of catalyst, especially the Brønsted acid sites, and affect the chemical state of Ru and low the cracking property of catalyst. But the carbon support pretreated by nitric acid presented a change of porous structure, graphitization of carbon support and reduced N groups. These findings were important to understand the catalytic mechanism for the HDO of biomass polyol

and provide guidance for the design of new catalytic formulations.

Acknowledgements This study was supported by grants from the National key research plan (2018YFB0604500), China Postdoctoral Science Foundation (207500), Scientific and Technological Research Projects of Henan Province (182102210319), Henan Polytechnic University (B2018-42), Outstanding Youth Foundation for Scientific and Technological Innovation in Henan Province (184100510013) and National Natural Science Foundation of China (51536009).

Compliance with ethical standards

Conflict of interest The authors declare that they have no conflict of interest.

References

1. Nakagawa Y, Liu S, Tamura M, Tomishige K (2015) Catalytic total hydrodeoxygenation of biomass-derived polyfunctionalized substrates to alkanes. *Chemsuschem* 8:1114–1132
2. Tomishige K, Tamura M, Nakagawa Y (2014) Role of Re species and acid cocatalyst on Ir-ReO_x/SiO₂ in the C–O hydrogenolysis of biomass-derived substrates. *Chem Rec* 14:1041–1054
3. Tomishige K, Nakagawa Y, Tamura M (2017) Selective hydrogenolysis and hydrogenation using metal catalysts directly modified with metal oxide species. *Green Chem* 19:2876–2924
4. Corma A, Iborra S, Velty A (2007) Chemical routes for the transformation of biomass into chemicals. *Chem Rev* 107:2411–2502
5. Wade JLG (2005) *Organic_Chemistry*. Prentice Hall, Upper Saddle River
6. Tomishige K, Nakagawa Y, Tamura M (2014) Selective hydrogenolysis of C–O bonds using the interaction of the catalyst surface and OH groups. In: Nicholas KM (ed) *Selective catalysis for renewable feedstocks and chemicals*. Springer, Berlin, pp 127–162
7. Alcalá R, Mavrikakis M, Dumesic JA (2003) DFT studies for cleavage of C–C and C–O bonds in surface species derived from ethanol on Pt(111). *J Catal* 218:178–190
8. Kunkes EL, Gurbuz EI, Dumesic JA (2009) Vapour-phase C–C coupling reactions of biomass-derived oxygenates over Pd/CeZrO_x catalysts. *J Catal* 266:236–249
9. Chen KY, Tamura M, Yuan ZL, Nakagawa Y, Tomishige K (2013) One-pot conversion of sugar and sugar polyols to n-alkanes without C–C dissociation over the Ir-ReO_x/SiO₂ catalyst combined with H-ZSM-5. *Chemsuschem* 6:613–621
10. Liu S, Okuyama Y, Tamura M, Nakagawa Y, Imai A, Tomishige K (2015) Production of renewable hexanols from mechanocatalytically depolymerized cellulose by using Ir-ReO_x/SiO₂ catalyst. *Chemsuschem* 8:628–635
11. Liu S, Okuyama Y, Tamura M, Nakagawa Y, Imai A, Tomishige K (2016) Catalytic conversion of sorbitol to gasoline-ranged products without external hydrogen over Pt-modified Ir-ReO_x/SiO₂. *Catal Today* 269:122–131
12. Zanutelio C, Landers R, Carvalho WA, Gomez Cobo AJ (2011) Carbon support treatment effect on Ru/C catalyst performance for benzene partial hydrogenation. *Appl Catal A Gen* 409:174–180
13. Huber GW, Cortright RD, Dumesic JA (2004) Renewable alkanes by aqueous-phase reforming of biomass-derived oxygenates. *Angew Chem* 43:1549–1551
14. Huber GW, Dumesic JA (2006) An overview of aqueous-phase catalytic processes for production of hydrogen and alkanes in a biorefinery. *Catal Today* 111:119–132
15. Kunkes EL, Simonetti DA, West RM, Serrano-Ruiz JC, Gartner CA, Dumesic JA (2008) Catalytic conversion of biomass to monofunctional hydrocarbons and targeted liquid-fuel classes. *Science* 322:417–421
16. Sener C, Wesley TS, Alba-Rubio AC, Kumbhalkar MD, Hakim SH, Ribeiro FH, Miller JT, Dumesic JA (2016) PtMo bimetallic catalysts synthesized by controlled surface reactions for water gas shift. *ACS Catal* 6:1334–1344
17. Shinmi Y, Koso S, Kubota T, Nakagawa Y, Tomishige K (2010) Modification of Rh/SiO₂ catalyst for the hydrogenolysis of glycerol in water. *Appl Catal B Environ* 94:318–326
18. Shimao A, Koso S, Ueda N, Shinmi Y, Furikado I, Tomishige K (2009) Promoting effect of Re addition to Rh/SiO₂ on glycerol hydrogenolysis. *Chem Lett* 38:540–541
19. Ota N, Tamura M, Nakagawa Y, Okumura K, Tomishige K (2016) Performance, structure, and mechanism of ReO_x-Pd/CeO₂ catalyst for simultaneous removal of vicinal OH groups with H₂. *ACS Catal* 6:3213–3226
20. Koso S, Watanabe H, Okumura K, Nakagawa Y, Tomishige K (2012) Comparative study of Rh-MoO_x and Rh-ReO_x supported on SiO₂ for the hydrogenolysis of ethers and polyols. *Appl Catal B Environ* 111–112:27–37
21. Qiu S, Wang T, Fang Y (2019) High-efficient preparation of gasoline-ranged C5–C6 alkanes from biomass-derived sugar polyols of sorbitol over Ru-MoO_{3-x}/C catalyst. *Fuel Process Technol* 183:19–26
22. Yang Y, Liu Q, Li D, Tan J, Zhang Q, Wang C, Ma L (2017) Selective hydrodeoxygenation of 5-hydroxymethylfurfural to 2,5-dimethylfuran on Ru-MoO_x/C catalysts. *RSC Adv* 7:16311–16318
23. Weng Y, Wang T, Duan P, Wang C, Wang F, Liu Q, Chen L, Wang H, Liang Z, Ma L (2018) Influence of impregnation processes on ruthenium-molybdenum carbon catalysts for selective hydrodeoxygenation of biomass sorbitol into renewable alkanes. *Energy Technol* 6:1763–1770
24. Weng Y, Wang T, Wang C, Liu Q, Zhang Y, Duan P, Wang L, Yin H, Liu S, Ma L (2018) Hydrodeoxygenation of sorbitol into bio-alkanes and -alcohols over phosphated ruthenium molybdenum catalysts. *ChemCatChem* 10:5032–5038
25. Weng Y, Wang T, Qiu S, Wang C, Ma L, Zhang Q, Chen L, Li Y, Sun F, Zhang Q (2017) Aqueous-phase hydrodeoxygenation of biomass sugar alcohol into renewable alkanes over a carbon-supported ruthenium with phosphoric acid catalytic system. *ChemCatChem* 9:774–781
26. Zhu X, Liu Y, Zhou C, Luo G, Zhang S, Chen J (2014) A novel porous carbon derived from hydrothermal carbon for efficient adsorption of tetracycline. *Carbon* 77:627–636
27. Ternero-Hidalgo JJ, Rosas JM, Palomo J, Valero-Romero MJ, Rodríguez-Mirasol J, Cordero T (2016) Functionalization of activated carbons by HNO₃ treatment: influence of phosphorus surface groups. *Carbon* 101:409–419
28. Dabbawala AA, Mishra DK, Huber GW, Hwang J-S (2015) Role of acid sites and selectivity correlation in solvent free liquid phase dehydration of sorbitol to isosorbide. *Appl Catal A* 492:252–261
29. Bedia J, Ruiz-Rosas R, Rodríguez-Mirasol J, Cordero T (2010) A kinetic study of 2-propanol dehydration on carbon acid catalysts. *J Catal* 271:33–42
30. Liu Y, Chen Z, Wang X, Liang Y, Yang X, Wang Z (2016) Highly selective and efficient rearrangement of biomass-derived furfural to cyclopentanone over interface-active Ru/carbon nanotubes catalyst in water. *ACS Sustain Chem Eng* 5:744–751
31. Sun F, Chen L, Weng Y, Wang T, Qiu S, Li Q, Wang C, Zhang Q, Ma L (2017) Transformation of biomass polyol into hydrocarbon fuels

- in aqueous medium over Ru–Mo/CNT catalyst. *Catal Commun* 99:30–33
32. Yao S, Zhang J, Shen D, Xiao R, Gu S, Zhao M, Liang J (2016) Removal of Pb(II) from water by the activated carbon modified by nitric acid under microwave heating. *J Colloid Interface Sci* 463:118–127
 33. Berenguer R, Ruiz-Rosas R, Gallardo A, Cazorla-Amorós D, Morallón E, Nishihara H, Kyotani T, Rodríguez-Mirasol J, Cordero T (2015) Enhanced electro-oxidation resistance of carbon electrodes induced by phosphorus surface groups. *Carbon* 95:681–689
 34. Guillén E, Rico R, López-Romero JM, Bedia J, Rosas JM, Rodríguez-Mirasol J, Cordero T (2009) Pd-activated carbon catalysts for hydrogenation and Suzuki reactions. *Appl Catal A* 368:113–120
 35. Liu Z-Q, Ma J, Cui Y-H, Zhao L, Zhang B-P (2010) Influence of different heat treatments on the surface properties and catalytic performance of carbon nanotube in ozonation. *Appl Catal B Environ* 101:74–80
 36. Al Bahri M, Calvo L, Gilarranz MA, Rodríguez JJ, Epron F (2013) Activated carbon supported metal catalysts for reduction of nitrate in water with high selectivity towards N_2 . *Appl Catal B* 138–139:141–148
 37. Weng Y, Qiu S, Wang C, Chen L, Yuan Z, Ding M, Zhang Q, Ma L, Wang T (2016) Optimization of renewable C5 and C6 alkane production from acidic biomass hydrolysate over Ru/C catalyst. *Fuel* 170:77–83
 38. Sassoie C, Muller G, Debecker DP, Karelavic A, Cassaignon S, Pizarro C, Ruiz P, Sanchez C (2011) A sustainable aqueous route to highly stable suspensions of monodispersed nano ruthenia. *Green Chem* 13:3230
 39. Fang R, Liu H, Luque R, Li Y (2015) Efficient and selective hydrogenation of biomass-derived furfural to cyclopentanone using Ru catalysts. *Green Chem* 17:4183–4188
 40. Tamura M, Tamura R, Takeda Y, Nakagawa Y, Tomishige K (2015) Insight into the mechanism of hydrogenation of amino acids to amino alcohols catalyzed by a heterogeneous $MoO_{(x)}$ -modified Rh catalyst. *Chem A Eur J* 21:3097–3107
 41. Weng Y, Qiu S, Ma L, Liu Q, Ding M, Zhang Q, Zhang Q, Wang T (2015) Jet-fuel range hydrocarbons from biomass-derived sorbitol over Ni-HZSM-5/SBA-15 catalyst. *Catalysts* 5:2147–2160
 42. Koso S, Ueda N, Shinmi Y, Okumura K, Kizuka T, Tomishige K (2009) Promoting effect of Mo on the hydrogenolysis of tetrahydrofurfuryl alcohol to 1,5-pentanediol over Rh/SiO₂. *J Catal* 267:89–92
 43. Takeda Y, Shoji T, Watanabe H, Tamura M, Nakagawa Y, Okumura K, Tomishige K (2015) Selective hydrogenation of lactic acid to 1,2-propanediol over highly active ruthenium-molybdenum oxide catalysts. *ChemSuschem* 8:1170–1178
 44. Chen L, Zhu Y, Zheng H, Zhang C, Li Y (2012) Aqueous-phase hydrodeoxygenation of propanoic acid over the Ru/ZrO₂ and Ru–Mo/ZrO₂ catalysts. *Appl Catal A* 411–412:95–104
 45. Wang W, Guo S, Lee I, Ahmed K, Zhong J, Favors Z, Zaera F, Ozkan M, Ozkan CS (2014) Hydrous ruthenium oxide nanoparticles anchored to graphene and carbon nanotube hybrid foam for supercapacitors. *Sci Rep* 4:4452
 46. Xiong H, Motchelaho MAM, Moyo M, Jewell LL, Coville NJ (2011) Correlating the preparation and performance of cobalt catalysts supported on carbon nanotubes and carbon spheres in the Fischer–Tropsch synthesis. *J Catal* 278:26–40
 47. Xiong H, Schwartz TJ, Andersen NI, Dumesic JA, Datye AK (2015) Graphitic-carbon layers on oxides: toward stable heterogeneous catalysts for biomass conversion reactions. *Angew Chem* 54:7939–7943
 48. Modestov AD, Tarasevich MR, Pu H (2012) Investigation of methanol electrooxidation on Pt and Pt–Ru in H₃PO₄ using MEA with PBI–H₃PO₄ membrane. *J Power Sources* 205:207–214
 49. Ikeda Y, Asadullah M, Fujimoto K, Tomishige K (2001) Structure of the active sites on H₃PO₄/ZrO₂ catalysts for dimethyl carbonate synthesis from methanol and carbon dioxide. *J Phys Chem B* 105:10653–10658
 50. Sun Y, Yue Q, Mao Y, Gao B, Gao Y, Huang L (2014) Enhanced adsorption of chromium onto activated carbon by microwave-assisted H₃PO₄ mixed with Fe/Al/Mn activation. *J Hazard Mater* 265:191–200
 51. Reffas A, Bernardet V, David B, Reinert L, Lehocine MB, Dubois M, Batisse N, Duclaux L (2010) Carbons prepared from coffee grounds by H₃PO₄ activation: characterization and adsorption of methylene blue and Nylosan Red N-2RBL. *J Hazard Mater* 175:779–788

Publisher's Note Springer Nature remains neutral with regard to jurisdictional claims in published maps and institutional affiliations.